Applied Surface Science 290 (2014) 482–489

Contents lists available at ScienceDirect

Applied Surface Science

journal homepage: www.elsevier.com/locate/apsusc

Microstructural stability of ultrafine grained cold sprayed 6061 aluminum alloy

M.R. Rokni[a,*], C.A. Widener[a], V.R. Champagne[b]

[a] Department of Materials & Metallurgical Engineering, Advanced Materials Processing Center, South Dakota School of Mines & Technology (SDSM&T), SD, USA

[b] U.S. Army Research Laboratory, Weapons and Materials Research Directorate, Aberdeen Proving Ground, MD, USA

ARTICLE INFO

Article history:
Received 27 August 2013
Accepted 23 November 2013
Available online 1 December 2013

Keywords:
Aluminum alloys
Cold spraying
Non-isothermal
Annealing
TEM

ABSTRACT

The microstructural stability of ultrafine grained (UFG) cold spray 6061 aluminum deposits produced by high pressure cold spray were investigated by in situ heating to a fully annealed state via a hot-stage transmission electron microscope (TEM). It was possible to observe the precise locations and temperatures of different microstructural changes, like dislocation movement and other restoration processes. Even after heating up to the annealing temperature for this alloy, the deposited layer in the perpendicular direction was found to preserve the UFG structures, which were the result of different recrystallization mechanisms caused by the high strains present during cold spraying. Extensive solute segregation at the grain boundaries acted as an obstruction for grain boundary migration in this direction, thereby preventing grain growth. However, in the direction parallel to the deposited surface, the UFGs were not resistant to grain coursing like the other direction, since the grain boundaries had much less solute segregation.

1. Introduction

Recently, considerable efforts have been devoted to fabricate bulk ultrafine grained (UFG) materials without porosity and a better combination of ductility and strength by imposing severe plastic strain [1–6]. A high degree of deformation coupled with the ability to tailor admixtures of powders during cold spraying (CS) can produce dense homogeneous or functionally graded microstructures unattainable by traditional P/M methods as well as UFG or even nano structure [5–7]. Often UFG and as-deformed structure, which is believed to be thermo-dynamically metastable due to excess amounts of various lattice defects and elastic distortions [8], can work together to provide excellent strength at room temperature, however, for many applications a more thermodynamically stable microstructure with better ductility would be preferred. Hence, thermally activated restoration processes, e.g. recovery, recrystallization and grain growth, that arise during annealing to high temperatures, are of interest here. In many cases, precisely controlled recovery and recrystallization of cold sprayed or severely deformed structures have been used to augment ultrafine grain formation [9–12].

There is also some indirect evidence of grain boundary (GB) segregation in UFG materials processed by cold work [13–17]. GB segregation is an extremely sensitive phenomenon because it may affect significantly material properties like corrosion resistance, mechanical behavior, or thermal stability [17–19]. It is thus of great importance to examine the mechanisms of the deformation-induced solute redistribution and concurrent grain boundary migration that was observed in the as-sprayed deposition of this investigation.

Non-isothermal heat treatments, especially the use of low heating rates, are frequently encountered during thermo-mechanical processing cycles, and hence are of importance for industrial purposes. During non-isothermal heat treatment, recovery and precipitation are likely to occur, generating complex interactions with recrystallization. Precipitation can also strongly influence the recrystallization behavior. The precipitation of dispersoids in the course of an annealing treatment can hinder or even suppress recrystallization [20–22]. Liu et al. [23] attributed the occurrence of large, inhomogeneous grain sizes in AA3105 to the occurrence of concurrent precipitation. Bampton et al. [20] also reported low heating rates should be employed in order to obtain maximum benefit from the fine grain processing technique. It has been demonstrated that the extent of recovery and precipitation also influence the recrystallization temperature [24].

The present study was undertaken in an effort to understand the recovery and recrystallization processes and associated changes in the microstructure during heating and annealing of a highly deformed 6061 alloy layer deposited by high pressure CS. Finding the exact temperatures for the processes involved during heating are important for microstructural control. In this case,

* Corresponding author. Tel.: +1 605 8776902; fax: +1 605 3945246.
E-mail addresses: mohammadreza.rokni@mines.sdsmt.edu, mreza.rokni@gmail.com (M.R. Rokni).

0169-4332/$ – see front matter © 2013 Elsevier B.V. All rights reserved.
http://dx.doi.org/10.1016/j.apsusc.2013.11.127

an in situ hot-stage TEM investigation was found to be a suitable and powerful tool to study and probe the complex interactions and thermal stability of the various inhomogeneous as-deposited microstructures, during non-isothermal heating and annealing.

2. Experimental procedure

In the present study, a 6061 coating was produced with a commercial gas-atomized 6061 Al powder as the feed stock with a size range of 5–50 μm and an average size of 38.7 μm (measured with Microtrac S3000 instrument). Helium was used as the process gas to achieve high impact between incident particles. The deposits were made using a CGT 4000 cold spray system and the pressure and temperature of helium were maintained at 28 bar and 400 °C, respectively. The deposit was made up to reach a total thickness of 10 mm.

The powder morphology and the coating microstructure were examined using SEM samples, sectioned for both the *Z* direction (looking into the deposit parallel to the direction of impact) and the *Y* direction (perpendicular to the impact and in the plane of the deposit). The microstructure of the coatings was also analyzed by TEM using a JEM-2100 LaB_6 equipped with a hot-stage and energy dispersive X-ray spectroscopy (EDX) analysis, using discs of 3 mm diameter punched from different directions of the coating, and then polished, dimpled, and ion milled for 4 h.

The annealing behavior of the cold spray deposited material was characterized by continuous in situ heating of the sample to 450 °C in 45 min (10 °C/min) from ambient temperature using the TEM heating stage followed by microstructural characterization in the Z and *Y* directions. A custom software code was written to take an image from the microstructure every 5 s in order to make a movie of the whole heat treatment. As a result, all of the notable microstructural changes, like the temperatures at which dislocations started to move, precipitation, recovery and recrystallization, were observed and recorded.

Thermal analysis was also performed in a SDT Q600 differential scanning calorimeter (DSC) in order to investigate the phase evolution of 6061 deposited sample during the continuous heating. Polished alloy disks with a diameter of 3 mm were sealed in Al pans and heated in a flowing Argon atmosphere at the same heating rate used in the TEM. Two DSC runs were successively performed on each sample with the curve from the second run used as the baseline.

3. Results and discussion

3.1. As-received 6061 Al powder

3.1.1. Morphology and microstructure

Fig. 1 shows the microstructure of the feedstock powder in which the spherical shape and size range of particles can be seen. Fig. 1(a), clearly depicts a typical particle size in the range of ~35 μm for the as-received 6061 Al powder particle. In Fig. 1(b) the grain structure of the as-received powder can be observed. According to this image scale, the powder structure consists of grains and subgrains in the range of 1–4 μm. TEM image of the powder in Fig. 1(c) demonstrates the presence of subgrain structures and dislocations in the powder particles. As seen in this figure, the subgrains are in the size range of ~200 nm, which some authors suggest can later transform into ones with well-defined low angle grain boundaries (LAGBs) after cold spray processing [6,25,26].

3.1.2. Phase identification and solute segregation

The back scattered SEM image in Fig. 2(a) confirms the same grain structure observed on the surface is also present inside of the powder particles. As can be seen, the GBs have a different chemical composition compared with matrix, which is evidence of solute segregation in the particles. The EDS analysis of the as-atomized 6061 powder (Fig. 2(b)) shows that the GBs in the powder particles are rich in Si, Mg, Cu and Fe elements. Different compositions of GB

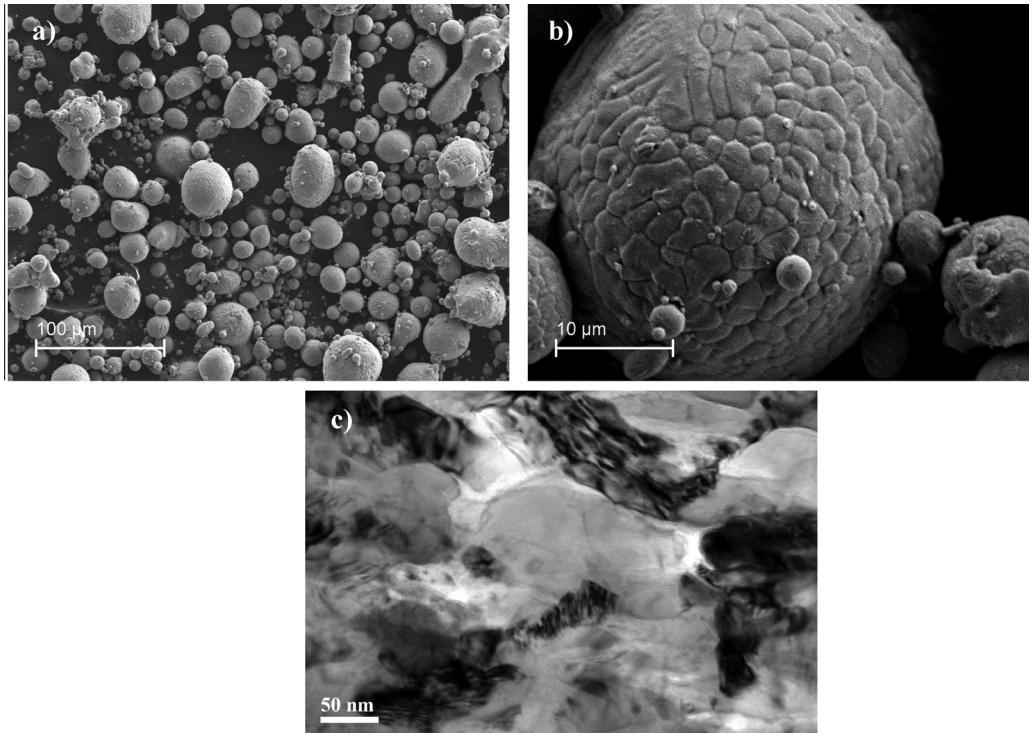

Fig. 1. Images from as-received 6061 Al powder. (a) SEM micrograph about powder morphology, (b) SEM micrograph showing the grain structure of the powder and (c) TEM image showing the presence of subgrain structures and dislocations in the powder particles.

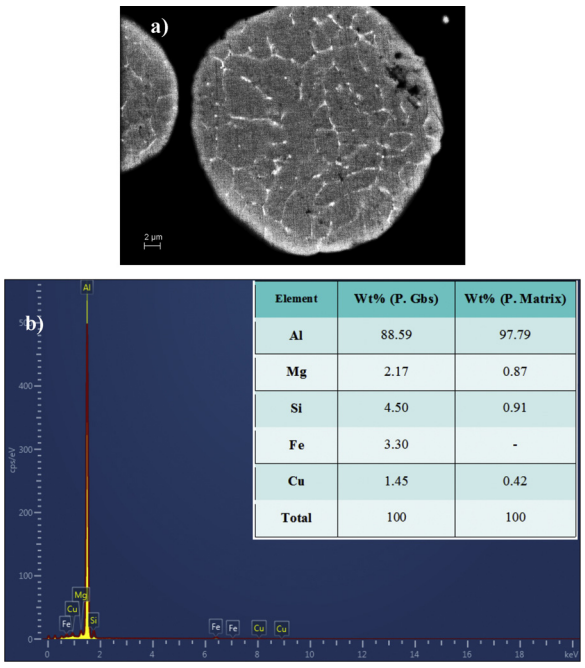

Element	Wt% (P. Gbs)	Wt% (P. Matrix)
Al	88.59	97.79
Mg	2.17	0.87
Si	4.50	0.91
Fe	3.30	-
Cu	1.45	0.42
Total	100	100

Fig. 2. (a) Back-scattered image showing the solute segregation at GBs of powder particles and (b) the EDS analysis comparison between of the as-atomized 6061 powder GB and matrix.

and matrix have been tabulated in the inserted table in Fig. 2(b). This solute segregation can be related to the nature of the powder producing procedure. Since atomized powder is produced by very high solidification rates from liquid temperatures, but does not necessarily cool quickly below the solidus temperature, retained heat in the particles collected after solidification could allow for the solute elements to diffuse to the GBs.

3.2. Microstructural evolution of deposited layer

3.2.1. Grain structure and morphology

Fig. 3 shows a TEM image from the as-deposited 6061 layer in *Z* direction. Individual grains were produced with sizes ranging from less than 100 nm to a few hundred nanometers, separated by high-angle grain boundaries (HAGBs). Some grains are heavily strained and contain a high density of dislocations. Some of these dislocations inside the as-deposited layer can be attributed to the presence of dislocations in the as-received powder particles. It has also been well established that these dislocations can act as diffusion paths for solute atoms, and provide nucleation sites for precipitation during processing and post-heat treatment, respectively. Moreover,

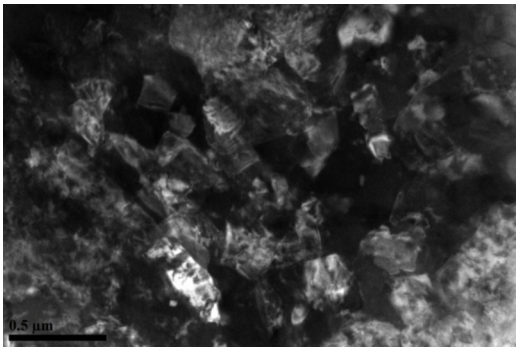

Fig. 3. TEM images from the 6061 deposited layer showing size range of individuals grains in *Z* direction.

since the as-received powder has dislocation structure or substructure inside, some of these subgrains can be the consequence of powders interacting with one another during deformation through geometric dynamic recrystallization (GDRX) [27–29].

3.2.2. Microstructure before heat treatment

Fig. 4 shows TEM images from the microstructure after cold spraying, from both the *Z* direction and the *Y* direction. The high-velocity impact of the powders created by high pressure cold spray causes large plastic deformations, which in turn yields much greater dislocation densities, and consequently more extensive recovery and crystallization at particle/particle interfaces in the deposit. As seen in Fig. 4(a), the grain size reduction in this area achieved by CS in the 6061 Al alloy was substantial, with nearly half of the grains now present below 100 nm. This overall is much finer that some other results previously reported in the literature [30]. As also seen in this figure, the grain boundaries are not clearly resolved and the diffraction contrast inside the grains is non-homogeneous. This indicates a high level of internal stress and elastic distortion of the crystal lattice. Such a complex contrast observed both inside the grains containing lattice dislocations and the grains having no defects testifies that grain boundaries are the source of the internal stress [8]. This indicates that the stresses are not internal to the grains from high dislocation density (DD), solute elements, precipitates, etc., but that this section of the microstructure is under a larger bulk residual stress, with those stresses being exerted on the grains at each boundary in the zone. TEM studies also revealed the presence of three types of ultra fine grains. In small grains, up to 100 nm in size, dislocations were almost absent, in grains of an intermediate size separate chaotically arranged dislocations were observed, and in large grains (over 200 nm) the formation of subgrains was revealed.

The TEM micrographs of the CSP layer in the *Y* direction are seen in Fig. 4(b) and (c), showing lamellar MBs with elongated nano grains inside and well-defined grain boundaries. Kikuchi analysis revealed that nearly all of the lamellar boundaries were high angle in character and they thus delineate long thin ribbon shaped grains. Some grains can be seen to extend almost across the entire figure and contain transverse HAGBs and LAGBs (arrows) with a spacing of 50–200 nm, producing a 'ladder-like', or 'bamboo', structure, which is a common microstructural feature in cold worked materials [16,31]. The absorption of dislocations into transverse boundaries and dislocations pile up behind these boundaries were also observed in certain places (dashed circles in Fig. 4(c)).

3.2.3. Micro-segregation of solute elements

Fig. 5 shows EDS micrographs from the CSP 6061 deposited layer in the *Y* direction illustrating the occurrence of solute segregation at the grain boundaries. In many large-grain alloys, solute segregation to the grain boundaries embrittles the material (e.g. Si segregation to the grain boundaries of Fe, and S segregation to the grain boundaries of Ni). According to EDS analysis, there are Si, Cu, Mg and Fe rich precipitates which are preferentially distributed at the GBs. Compared with the as-received powder particles, more extensive solute segregation has been observed after CS (Table 1), which is explained below.

The solute segregation observed here has a similar corollary in irradiated materials from a vacancy transport mechanism. Kinetic solute segregation, as a consequence of a radiation-induced vacancy flow, has been suggested by Anthony [32]. He considered two mechanisms. The first results from preferential exchange of substitutional alloying elements with vacancies, which leads to a preferential flow of the alloying elements in the opposite direction of the vacancy flow. The second mechanism results from a strong binding between alloying elements and vacancies, which causes a 'dragging' of this alloying element in the same direction as the

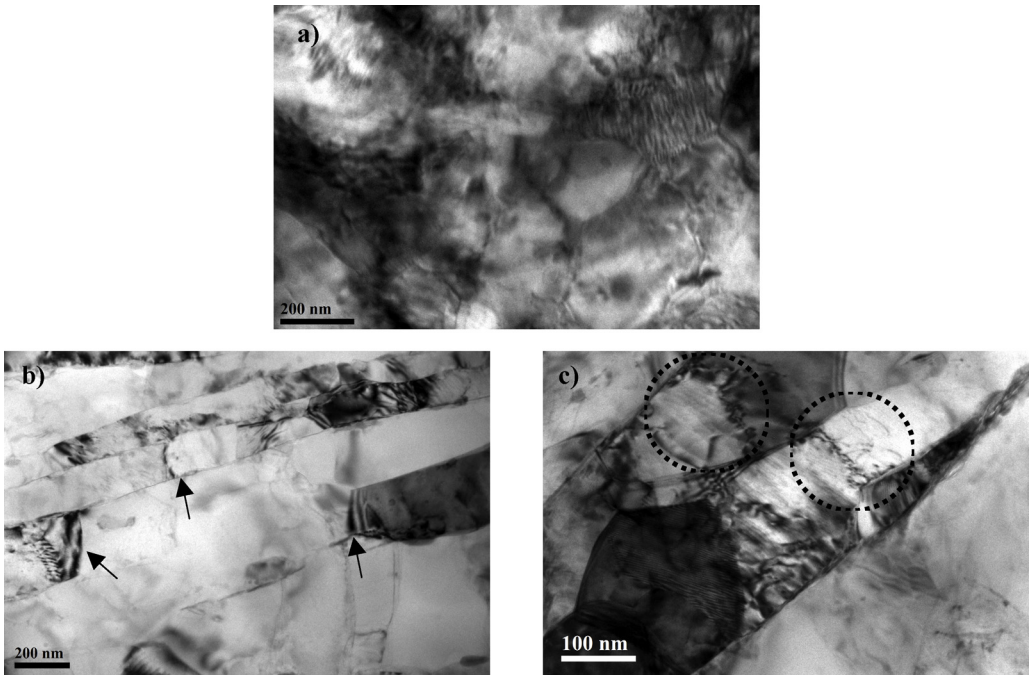

Fig. 4. TEM images from the as-sprayed deposition layer in different directions: (a) nano recrystallization along *Z* direction and (b and c) lamellar microbands and elongated nano grains inside along *Y* direction.

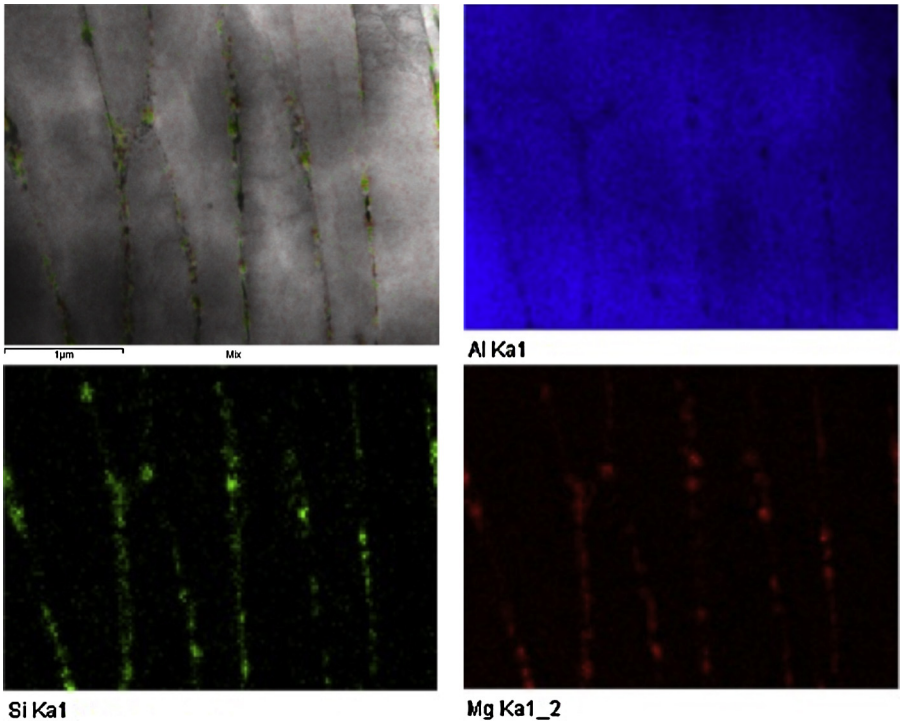

Fig. 5. EDS micrographs from the 6061 deposited layer showing Mg and Si segregation at GBs.

vacancy flow. The two mechanisms may oppose or supplement each other in producing segregation. The question arises: can CS produce additional vacancies for acceleration of diffusion, similar to those produced by the irradiation of materials?

Early estimations of the vacancy production during cold work were made based on the data for residual resistivity measurements [33]. In metals the residual resistivity attributed to point defects increases with the strain ε according to the laws which vary somewhat with the type of the stress-strain curve. From the residual resistivity per Frenkel pair, deduced from irradiation experiments, it was concluded that atomic concentrations of 10^{-5} to 10^{-4} are reached for strains $\varepsilon \sim 1$ [34,35]. Therefore, even a strain of $\varepsilon \sim 1$ produces the vacancy concentration comparable to the equilibrium value at the melting point (about 10^{-4} [33]). The recombination of the dislocations other than screws placed in neighboring parallel planes has been considered as a most possible mechanism for the vacancy production [33]. Since it is well established that atomic concentration c of point defects can be predicted from $c \sim 10^{-4}\varepsilon^2$,

Table 1
The results of EDS analyses on the powder grain boundary and matrix and cold sprayed deposition matrix proving more solute segregation after cold spraying.

Element	wt% (P. GBs)	wt% (P. matrix)	wt% (deposition matrix)
Al	88.59	97.79	99.3
Mg	2.17	0.87	0.7
Si	4.50	0.91	–
Fe	3.30	–	–
Cu	1.45	0.42	–
Total	100	100	100

for our case ($\varepsilon \sim 6$ [11,36]) results in high total vacancy production during the deformation process. Therefore, during CS a great number of dislocations and vacancies (point defects) are developed so that the CS-introduced defect concentration is very high compared with thermal equilibrium [25,31,36]. As a result, these excess point defects form defect clusters and/or migrate to defect sink sites such as grain boundaries. Thus, there is a flow of CS-introduced point defects toward boundary sinks during cold spraying. While this seems likely, a more detailed investigation would have to be conducted before drawing any reliable conclusions. For now, it suffices to say that in the CSP 6061 layer, a combination of mechanisms that assist diffusion through defects (dislocation and vacancy) are believed to be the primary explanation for the degree of solute segregation observed here.

3.3. Heat treatment of the CSP layer

3.3.1. Microstructure after heat treatment

The TEM micrographs of the *Z* and *Y* directions of the 6061 deposited layer after annealing to 450 °C with a 10° C/min heating rate are shown in Fig. 6(a) and (b), respectively. The annealing process involves the loss of some of the stored energy, which provides the driving force for recovery and recrystallization and the corresponding changes in the microstructure.

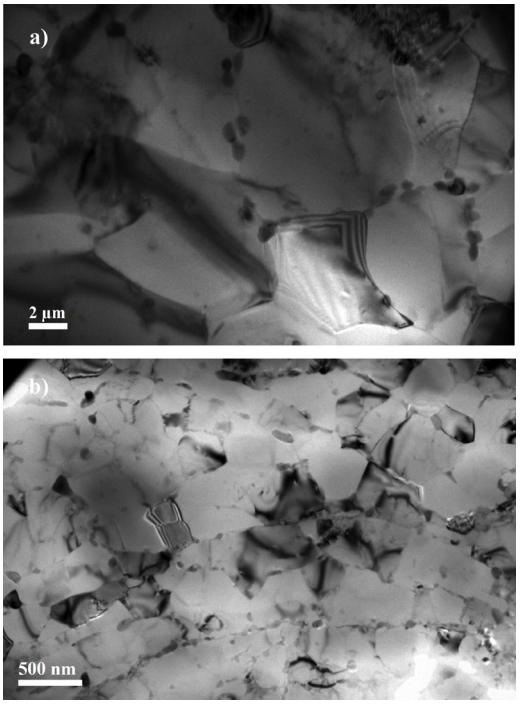

Fig. 6. TEM images from the cold spray deposition after heat treatment to 450 °C, (a) in *Z* direction and (b) in *Y* direction.

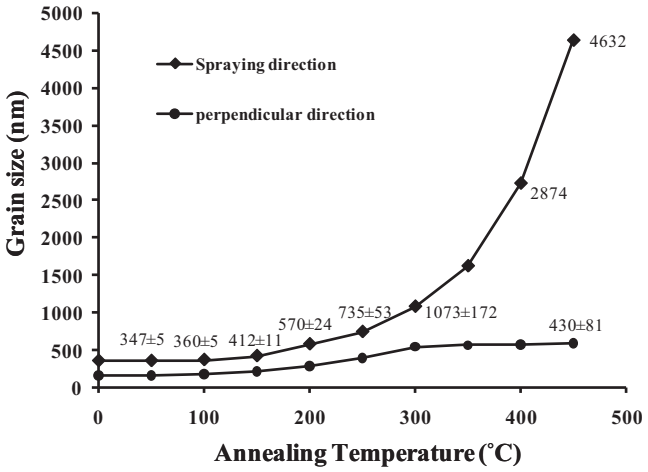

Fig. 7. Grain size variation with annealing temperature along both *Z* and *Y* directions.

The microstructure of the planar view (*Z* direction) annealed to 450° C is shown in Fig. 6(a). It reveals that the grains in the annealed CSP layer are equiaxed with well-defined straight grain boundaries unlike the inhomogeneous microstructure observed in the CSP coating. Additionally, the banded contrast observed in this image indicates that the boundaries are in equilibrium. Generation of the grain boundaries and the clarity of the TEM image indicate that residual stresses are relieved with the formation of interfaces and grains in the microstructure.

Fig. 6(b) shows a TEM image from the transverse direction of the 6061 CSP deposited layer after the heat treatment. While its microstructure after CS and prior to annealing contained a high fraction of non-equilibrium grain boundaries and a high inherent DD, the thermal activation during annealing facilitated restoration processes. As seen in these figures, the average grain size in the *Y* direction is much lower than the *Z* direction, which has been attributed to a high level of solute segregation in this direction. Wang et al. [37] and Aust et al. [38] have shown that the rate of grain boundary migration could be reduced dramatically even by small average solute concentrations. The latter also proved that the drag force increases with increasing boundary velocity at small velocities and it decreases with increasing velocity at large velocities. For this study, the heating rate was relatively low, and would not have provided a high driving force for grain boundaries to migrate. Consequently, the heating rate employed is believed to have kept GB velocities small by maintaining a high drag force.

Results of the grain size variation with annealing temperature along both directions, parallel and perpendicular to the cold

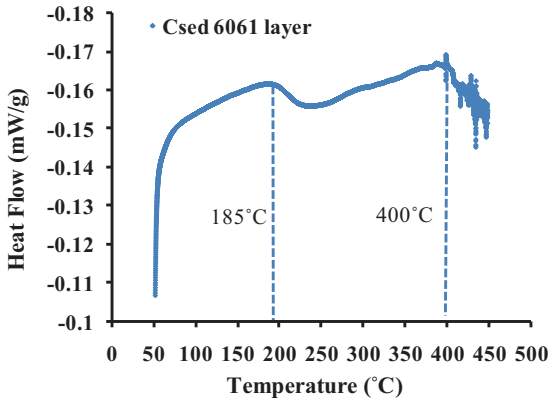

Fig. 8. DSC curve of the 6061 CS deposited layer. DSC scanning rate was set at 10 °C/min.

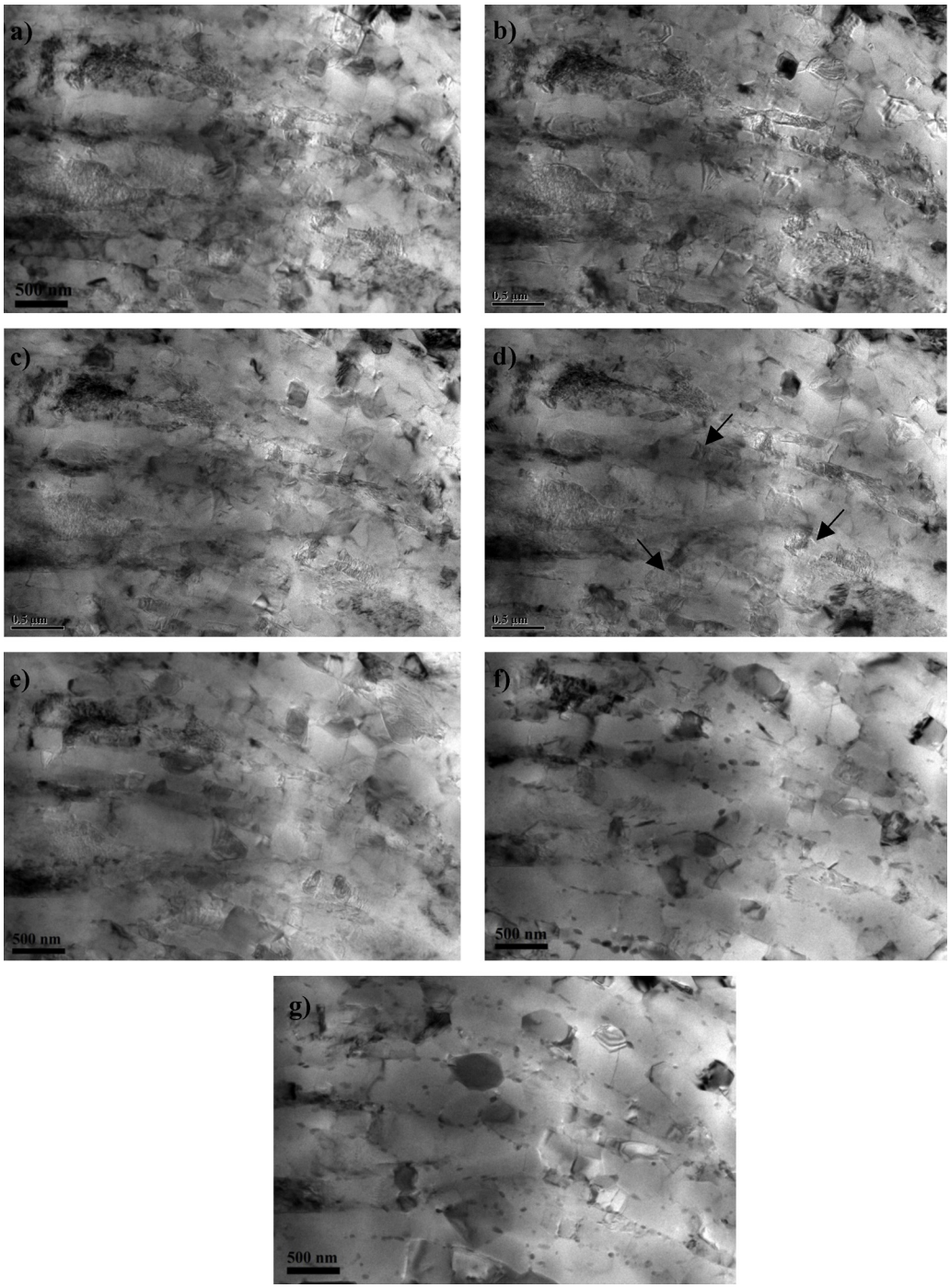

Fig. 9. TEM images from the heat treatment of the CSP 6061 layer in *Y* direction: (a) microstructure after CS processing, (b) 100 °C: few observable changes in the microstructure, (c) 150 °C: some evidence of recovery in the microstructure, (d) 200 °C: reduction in the average grain length, (e) microstructure of recrystallized grains at 300 °C, (f) precipitation mainly at GBs at 400 °C and (g) final microstructure at 450 °C.

spraying direction, are presented in Fig. 7. The curves show a continual increase in grain size with increasing annealing temperature, in both directions. This suggests that this material exhibits continuous growth and does not have an apparent conventional recrystallization stage. Such an observation is confirmed by DSC test results for the CSP sample. The DSC results, presented in Fig. 8, show no apparent exothermic peaks along the temperature range, which suggests the process of traditional nucleation is not present.

3.3.2. Microstructure evaluation during heat treatment

The full heat treatment cycle from room temperature to 450 °C (10 °C/min), with all of the observed microstructural changes (dislocation movement, recovery, precipitation and recrystallization) and their exact temperatures, was recorded in a movie file (Video). The time lapse movie is made up of about 650 TEM images that were taken every 5 s. In this way, the temperatures at which real microstructural changes actually begin can be observed. Select images have also been extracted and reproduced here. Fig. 9 shows a series of TEM images from in situ annealing of the 6061 deposited layer in the *Y* direction. There were few observable changes in the microstructure below 100 °C (Fig. 9(b); however, dislocation movement began as low as 70 °C. Annealing below this temperature would be expected to have little effect, as boundary mobility is very low.

On increasing the annealing temperature to 150 °C (Fig. 9(c)), boundary migration became more significant. There is also some evidence of recovery in the microstructure. Since the dislocation cell structure is not thermodynamically stable, the dislocations become more mobile and can annihilate to a reach a more strain-free state. It is also observable that the structure is beginning to equilibrate surface tensions by the lamella HAGBs of the elongated grains becoming bowed, where they are cross-linked by transverse LAGBs.

In Fig. 9(d), it can be seen that the average grain length has been reduced at 200 °C. This initial reduction in grain length and aspect ratio is driven by local imbalances in surface tension from the transverse LAGBs, causing the lamellar HAGBs to pinch-off and subdivide the ribbon grains into shorter segments (black arrows). DSC results in Fig. 8. Show there is exothermic peak temperature providing evidence that we also have precipitation around this temperature. Dunlop et al. [39] proved that these precipitates contain both Mg and Si with a ratio close to 1. This phenomenon is expected since Mg and Si atoms are segregated at GBs during CS.

According to our observations recrystallization starts at 300 °C (Fig. 9(e)), before there is significant precipitation, mainly in regions of the microstructure with the highest stored energies or very mobile boundaries. Recrystallized grains at this temperature are dislocation free and the grain boundaries appeared well defined and free of defects. It was also revealed that at this temperature the lamellar structure tends to collapse and ultra-fine grains form by a recrystallization and growth mechanism.

Increasing the annealing temperature to 400 °C (Fig. 9(f)) resulted in an additional increase in the average grain width and the grain aspect ratio continued to reduce. In accordance with the DSC results, we have more precipitation around this temperature initiated on the recovered substructure and established with a very high velocity due to GB segregation (from higher local supersaturation of precipitate-forming elements at GBs). Massive solute segregation at the GBs accompanying the heat treatment cycle caused the precipitates to nucleate and grow at these sites throughout the microstructure. As a result, the present precipitates appear to have a strong effect on grain growth (GG), presumably by pinning of the GBs.

As a result, even at high annealing temperatures, e.g. 440–450 °C, recrystallization proceeded relatively slowly because the movement of the recrystallization front is controlled by particle coarsening (Fig. 9(g)). Consequently, the recrystallized grains in some regions are still elongated owing to the Zener pinning arising from the precipitates on the prior high angle boundaries which are aligned in the GBs and which therefore inhibit grain growth.

4. Conclusions

The cold sprayed 6061 aluminum deposits produced by high pressure cold spray were investigated by different electron microscopies. Compared with the as-received powder particles, an increase in solute segregation was observed after CS, which has been attributed to the flow of solute elements through CS-introduced point defects (dislocations and vacancies). In order to investigate the microstructural stability of the CSP layer, a full heat treatment cycle from room temperature to 450 °C (10 °C/min) was also carried out using an in situ hot-state TEM. In this way, it was possible to observe the full recovery, recrystallization and grain growth process in the coating, both parallel (*Z*) and perpendicular (*Y*) to the direction of deposition. The microstructure of the *Z* direction annealed to 450 °C showed recrystallization and grain growth (equiaxed grains with well defined straight grain boundaries), however, the CSP coating was found to retain UFG structures in the *Y* direction, even upon heat treatment up to 450 °C, owing to the presence of solute segregation and precipitates at the GBs. All of the observed microstructural changes (dislocation movement and annihilation, recovery, precipitation and recrystallization) in the *Y* direction and their temperatures of their transformations were also recorded in a movie file.

Appendix A. Supplementary data

Supplementary data associated with this article can be found, in the online version, at http://dx.doi.org/10.1016/j.apsusc.2013.11.127.

References

[1] Y. Saito, N. Tsuji, H. Utsunomiya, T. Sakai, R.G. Hong, Ultra-fine grained bulk aluminum produced by accumulative roll-bonding (ARB) process, Scr. Mater. 39 (1998) 1221.
[2] V.M. Segal, Materials processing by simple shear, Mater. Sci. Eng. A 197 (1995) 157.
[3] R.Z. Valiev, R.R. Mulyukov, V.V. Ovchinnikov, V.A. Shabashov, Mossbauer analysis of submicrometer grained iron, Scr. Metall. Mater. 25 (1991) 2717.
[4] Y. Wang, M. Chen, F. Zhou, E. Ma, High tensile ductility in a nanostructured metal, Nature 419 (2002) 912–915.
[5] V.K. Champagne, The Cold Spray Materials Deposition Process: Fundamentals and Applications, Woodhead Publishing Limited, Cambridge, 2007.
[6] Y. Zou, D. Goldbaum, J.A. Szpunar, S. Yue, Microstructure and nanohardness of cold-sprayed coatings: electron backscattered diffraction and nanoindentation studies, Scr. Mater. 62 (2010) 395–398.
[7] K. Kim, M. Watanabe, J. Kawakita, S. Kuroda, Grain refinement in a single titanium powder particle impacted at high velocity, Scr. Mater. 59 (2008) 768.
[8] R.Z. Valiev, R.K. Islamgaliev, I.V. Alexandrov, Bulk nanostructured materials from severe plastic deformation, Prog. Mater. Sci. 45 (2000) 103–189.
[9] P.D. Eason, S.C. Kennett, T.J. Eden, I. Krull, B. Kowalski, J.L. Jones, In situ observation of microstrain relief in cold-sprayed bulk copper during thermal annealing, Scr. Mater. 67 (2012) 791–794.
[10] B. Poorganji, P. Sepehrband, H. Jin, S. Esmaeili, Effect of cold work and non-isothermal annealing on the recrystallization behavior and texture evolution of a precipitation-hardenable aluminum alloy, Scr. Mater. 63 (2010) 1157–1160.
[11] H. Assadi, F. Gärtner, T. Stoltenhoff, H. Kreye, Bonding mechanism in cold gas spraying, Acta Mater. 51 (2003) 4379–4394.
[12] K.T. Park, H.J. Kwon, W.J. Kim, Y.S. Kim, Microstructural characteristics and thermal stability of ultrafine grained 6061 Al alloy fabricated by accumulative roll bonding process, Mater. Sci. Eng. A 316 (2001) 145–152.
[13] T.W. Heo, S. Bhattacharyya, L.Q. Chen, A phase field study of strain energy effects on solute–grain boundary interactions, Acta Mater. 59 (2011) 7800–7815.
[14] J. Schäfer, A. Stukowski, K. Albe, Plastic deformation of nanocrystalline Pd–Au alloys: on the interplay of grain boundary solute segregation, fault energies and grain size, Acta Mater. 59 (2011) 2957–2968.
[15] X. Sauvage, Y. Ivanisenko, The role of carbon segregation on nanocrystallisation of pearlitic steels processed by severe plastic deformation, Mater. Sci. 42 (2007) 1615.
[16] P.B. Prangnell, J.S. Hayes, J.R. Bowen, P.J. Apps, P.S. Bate, Continuous recrystallisation of lamellar deformation structures produced by severe deformation, Acta Mater. 52 (2004) 3193–3206.
[17] C.C. Koch, R.O. Scattergood, K.A. Darling, J.E. Semones, Stabilization of nanocrystalline grain sizes by solute additions, Mater. Sci. 43 (2008) 7264–7272.
[18] R. Kirchheim, Reducing grain boundary, dislocation line and vacancy formation energies by solute segregation. I. Theoretical background, Acta Mater. 55 (2007) 5129–5138.
[19] R. Kirchheim, Reducing grain boundary, dislocation line and vacancy formation energies by solute segregation: II. Experimental evidence and consequences, Acta Mater. 55 (2007) 5139–5148.
[20] C.C. Bampton, J.A. Wert, M.W. Mahoney, Heating rate effects on recrystallized grain size in two Al–Zn–Mg–Cu alloys, Metall. Trans. A 13 (1982) 193.
[21] O. Daaland, E. Nes, Recrystallization texture development in commercial Al–Mn–Mg alloys, Acta Mater. 44 (1996) 1413.
[22] M. Somerday, F.J. Humphreys, Recrystallisation behaviour of supersaturated Al–Mn alloys. Part 1. Al–1.3 wt-% Mn, Mater. Sci. Technol. 19 (2003) 20.
[23] W.C. Liu, Z. Li, C.S. Man, Effect of heating rate on the microstructure and texture of continuous cast AA 3105 aluminum alloy, Mater. Sci. Eng. A 478 (2008) 173.
[24] R.A. Vandermeer, P. Gordon, The influence of recovery on recrystallization in aluminum, in: L. Himmel (Ed.), Recovery and Recrystallization of Metals, Gordon and Breach Science, NY, 1963.
[25] Y. Zou, W. Qin, E. Irissou, J.G. Legoux, S. Yue, J.A. Szpunar, Dynamic recrystallization in the particle/particle interfacial region of cold-sprayed nickel coating: electron backscatter diffraction characterization, Scr. Mater. 61 (2009) 899–902.
[26] G.R. Canova, C. Fressengeas, A. Molinari, U.F. Kocks, Effect of rate sensitivity on slip system activity and lattice rotation, Acta Metall. 36 (1988) 1961–1970.

[27] F.J. Humphreys, M. Hatherly, Recrystallization and Related Annealing Phenomena, 2nd ed., Pergamon Press, Oxford, 2004.
[28] M.R. Rokni, A. Zarei-Hanzaki, H.R. Abedi, Microstructure evolution and mechanical properties of back extruded 7075 aluminum alloy at elevated temperatures, Mater. Sci. Eng. A 532 (2012) 593–600.
[29] M.R. Rokni, A. Zarei-Hanzaki, A.A. Roostaei, H.R. Abedi, An investigation into the hot deformation characteristics of 7075 aluminum alloy, Mater. Des. 32 (2011) 2339–2344.
[30] K. Balani, A. Agarwal, S. Seal, J. Karthikeyan, Transmission electron microscopy of cold sprayed 1100 aluminum coating, Scr. Mater. 53 (2005) 845–850.
[31] L. Ajdelsztajn, A. Zúñiga, B. Jodoin, E.J. Lavernia, Cold gas dynamic spraying of a high temperature Al alloy, Surf. Coat. Technol. 201 (2006) 2109–2116.
[32] T.R. Anthony, Radiation-induced voids in metals and alloys, in: J.W. Corbett, L.C. Lanniello (Eds.), AEC Syrup. Series, Conf-701601, 1972.
[33] J. Friedel, Dislocations, Pergamon Press, Oxford, 1964.
[34] B. Straumal, R. Valiev, O. Kogtenkova, P. Zieba, T. Czeppe, E. Bielanska, M. Faryna, Thermal evolution and grain boundary phase transformations in severely deformed nanograined Al–Zn alloys, Acta Mater. 56 (2008) 6123–6131.
[35] B.B. Straumal, B. Baretzky, A.A. Mazilkin, F. Phillipp, O.A. Kogtenkova, M.N. Volkov, R.Z. Valiev, Formation of nanograined structure and decomposition of supersaturated solid solution during high pressure torsion of Al–Zn and Al–Mg alloys, Acta Mater. 52 (2004) 4469–4478.
[36] C. Borchers, F. Gärtner, T. Stoltenhoff, H. Kreye, Formation of persistent dislocation loops by ultra-high strain-rate deformation during cold spraying, Acta Mater. 53 (2005) 2991–3000.
[37] N. Ma, S.A. Dregia, Y. Wang, Solute segregation transition and drag force on grain boundaries, Acta Mater. 51 (2003) 3687–3700.
[38] J.W. Rutter, K.T. Aust, Trans. AIME 218 (1960) 682.
[39] G.A. Edwards, K. Stiller, G.L. Dunlop, M.J. Couper, The precipitation sequence in Al–Mg–Si alloys, Acta Mater. 46 (1998) 3893–3904.